Indian Journal of Pure & Applied Physics
Vol. 64, May 2026, pp. 534-546
DOI: 10.56042/ijpap.v65i5.27666

# FEM-Based Analysis of Delay-Line SAW Resonator Sensors for Volatile Organic Compound Detection

Rudransh Soni[a], Raju Patel[a*], Chandramauleshwar Roy[a], Manoj Singh Adhikari[b] & Deepak Bansal[c]

[a]School of Electronics Engineering, Vellore Institute of Technology, Chennai 600 127, India
[b]Department of Computer Science and Engineering, Graphic Era Hill University, Haldwani 263 139, India
[c]CSIR-Central Electronics Engineering Research Institute, Pilani 333 031, India

*Received: 17th January 2026; accepted: 12th March 2026*

Surface Acoustic Wave (SAW) resonator sensors have high sensitivity and selectivity in sensing Volatile Organic Compounds (VOCs) using mass-loading effects on the sensing layer. This paper describes the design and Finite Element Method (FEM)-based analysis of a delay-line SAW resonator for VOC sensing, focusing on PCE detection using polyisobutylene (PIB) as the active sensing layer. The analysis begins by describing the basic properties, applications, and limitations of SAW filters, together with a categorization scheme for acoustic devices. A detailed discussion about the optimization of SAW sensors is provided through the piezoelectric substrate, material properties, and fine-tuning of the IDT. Further optimization extended to multiple types of IDTs, including selection of materials, delay length to improve the performance of the SAW device. The frequency domain analysis has been performed to obtain $S_{11}$ and displacement plot. The optimized SAW resonator used for VOC detection into the dynamic behavior of the filter. The proposed sensor was exposed to six organic gases, with their concentrations varying from 0 to 400 ppm. The frequency downshift of the SAW sensor was linear with the 400 ppm concentration of PCE gas, with a frequency shift (Δf) of 270 kHz and a calculated sensitivity of 0.67 kHz/ppm. The structure under consideration has simulated high selectivity for PCE gas, the sensor is designed for 158 MHz range. These important findings of the study make work highly useful for optimization or application in diversified technological domains to benefit researchers and engineers in this field.

**Keywords:** Surface acoustic waves, IDT, FEM, COMSOL multiphysics, VOC detection

## 1 Introduction

SAW technology, based on the piezoelectric principle, has gone through rapid advances since Lord Rayleigh's discovery in 1885. Applications of SAW technology in band-pass filters, resonators, oscillators, and compression filters have been extended to the sectors of telecommunications, MEMS, and biotechnology since the 1960s. The innovation was the application of planar surfaces for transducers by Rowen and Mortley in 1963; this changed focus from bulk waves to surface waves[1, 2]. White and Voltmer extended the field in 1965 by developing IDTs on piezoelectric substrates for efficient surface wave generation. SAW sensors are reliable, rugged, have passive wireless operation, and are cost-effective. They are compatible with semiconductor fabrication process that ensure high quality and scalability. The multi-layer substrate design with 42°Y-X $LiTaO_3/SiO_2$/poly-Si/Si comprises layers with various thicknesses per its design (1-5 μm) to achieve certain thermal/acoustic gradient profiles to entrap Surface Rayleigh Waves (SRW) to the substrate surface. The low velocity ($SiO_2$) and high velocity (Si) substrate ensure phase velocities 4000 m/s with a Bode Q 2000 and a bandwidth of 5 %. A flat slowness curve design allows for the predominate suppression of unwanted transverse modes and the separate layers provide inherently better thermal compensation than monolithic quartz substrates due to the differential thermal expansion of the layers[3]. Apodization of interdigital transducers (IDTs) employs windowing (Hamming, Blackman) techniques on overlapping electrodes to smoothly vary the width of overlapping electrodes within the aperture, thus reducing triple-transit interference and spurious sidelobes. The smoothly varying function enhances the focusing of acoustic waves along the centerline of the transducer, resulting in a 15-40 dB sidelobe reduction and a 3x increase in main-mode conductance compared to unweighted IDTs. Split-finger geometries, where odd

*Corresponding author: E-mail: raju.patel@vit.ac.in

and even electrodes are electrically separated to eliminate electromagnetic feed through and enable fundamental frequency operation up to 2 GHz without generation of any harmonic modes, with only small (1-2 dB) losses in transduction efficiency[4]. In the telecommunication industry, they correctly select and handle frequencies. Therefore, SAW device in Fig. 1, have low power operated and has been widely used in wireless communication, signal processing, mobile phones and industrial monitoring applications[5–9]. They are compact, reliable, and lightweight with the capability to process complex signals. Thus, high-performance, cost-effective products drive continual improvements to address the industry's need for compact energy-efficient components for many applications such as gas detection for VOCs[10].

VOCs are the volatile organic compounds, which readily evaporate at room temperature with wide distribution in industrial emissions, household products, and vehicle exhaust. They can be detected for the impact upon air quality, human health, and environmental safety. In gas sensing industry VOC detection is quite important to the monitoring of level of pollution in the environment with safety at workplace and prevention against hazardous exposure. The capability of trace-level detection with high accuracy, selectivity and rapid response depending on the deposition method and growth of sensing layer. Different types of gas sensing layer proposed by the researcher like, hybrid CuO@$V_2C$ *MXene*, and sulfur doped g-$C_3N_4$ quantum dots for the detection of $H_2S$ and $NH_3$ gas, respectively[11–13]. Surface Acoustic Wave (SAW) sensors promise to be quite promising in terms of VOC detection due to its high sensitivity as well as a real-time ability to monitor events and the simple operation without involving complex sample preparations. SAW-based gas sensors, by involving specific sensing layers, can thus selectively identify given VOCs to be highly useful for applications within environmental monitoring, industrial safety, and biomedical diagnostics[14, 15].

This paper presents a finite element method (FEM) analysis to enhance the performance of a SAW resonator by optimizing its delay line length. The optimized resonator is applied to VOC detection, incorporating a polymer sensing layer in the delay line region. Selectivity toward tetrachloroethylene (PCE) gas is further evaluated by simulating the sensor response in the presence of interfering gases.

## 2 Physics Behind SAW Device

Surface Acoustic Waves (SAWs) are a type of mechanical wave (Fig. 2), which propagate at the surface of the material, usually a piezoelectric substrate. The use of SAWs in modern technology includes applications in electronics, tele-communications, sensing devices, magnon microwave antenna, and reservoir computing[16, 17]. A SAW filter converts electrical energy into an acoustic wave that is modulated by such a device to permit certain specific frequencies to pass through device[18–20]. Interdigitated transducers (IDTs), which are deposited on a piezoelectric material, like quartz, lithium niobate, or lithium tantalate, convert electrical signals into acoustic waves.

The waves propagate in the medium and are always penetrating the substrate, leading to an insertion loss in the filter, consequently reducing the overall performance of the device. SAW devices support various types of surface waves, including Rayleigh

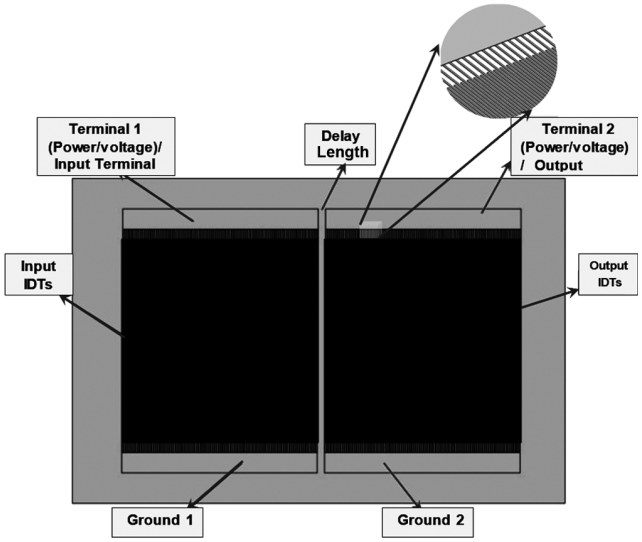


Fig. 1 — Basic Structure of a SAW Device

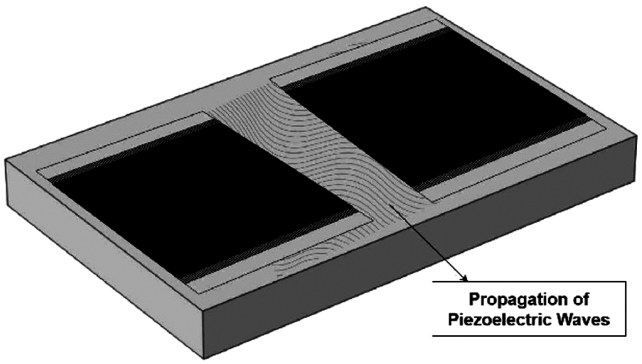


Fig. 2 — Propagation of piezoelectric waves in SAW Device

waves, which travel along the surface of the device but gradually diminish in intensity with increasing depth. The application of Rayleigh waves is widely utilized within the SAW sensors. SH waves travel perpendicular to the wave progression without amplitude loss. Lamb waves travel through the depth of a substrate, passing through structures that are similar to plates[21–23]. Love waves follow the boundary between two media that consist of solid materials and move horizontally[24]. The types of waves function differently in SAW devices. It generates resonant mode through the mechanical vibrations that propagate along the surface as acoustic waves when an electrical signal is subjected to the IDTs on a piezoelectric substrate.

Piezoelectric materials convert electrical signals into mechanical deformations through the inverse piezoelectric effect. In SAW filters, these mechanical deformations generate surface acoustic waves that propagate along the surface, carrying the signal information. The three basic components of SAW devices are a substrate, a piezoelectric layer, and IDTs. In this case, the substrate is the propagation medium, while the piezoelectric layer typically consists of material capable of converting electrical signals into mechanical vibrations and vice versa; commonly, it is zinc oxide. IDTs are interleaved arrays of electrodes that generate and detect surface acoustic waves.

There are several SAW device configurations. A SAW delay line, fabricated on a piezoelectric substrate, comprises two IDTs as illustrated in Fig. 1. When an electrical signal is applied to one IDT, it generates acoustic waves that travel across the substrate to the second IDT, where they are converted back into an electrical signal[16, 17]. A one-port resonator, used in telecommunication sensors and filters, has an IDT between two reflective gratings. Besides this, two-port resonators have a comparatively larger size since they have two IDTs and two reflectors. The devices exhibit another peak in the frequency response aside from the fundamental resonant peak. The variety of possible configurations makes SAW devices suitable for very broad signal-processing tasks with high efficiency.

## 3 Design of SAW Device

### 3.1 Mathematical Equations Required for Designing SAW

The Basic Structure of the SAW Device contains many parameters that define its performance. The IDT structure with the delay line configuration of a linear SAW Device is critical to operational efficiency. It features a central frequency determined by the spacing (or period) of the IDT fingers and the acoustic velocity of the substrate material, while the wavelength calculates the wavelength at which the device operates. The period is the distance that describes the delay line configuration, while the Finger Width and Spacing that govern wave propagation. The efficiency of energy conversion from electrical to acoustic and vice versa is improved with an increase in the number of finger pairs in the structure, enhancing power handling capability. The Null Bandwidth as stated defines the bandwidth and the range of frequencies wherein the signal is attenuated, depending on its application, for optimal filtering. Further, total static capacitance is the sum of capacitance present in the electrical parts of the device and, thus, alters the impedance behavior. Aperture refers to the effective width of Interdigitated Transducers; hence, their interaction with Surface Acoustic Wave (SAW) will be altered. The coupling coefficient is one that measures energy conversion efficiency; it is important in the confinement of surface wave on the device. Finally, the capacitance per unit length between a pair of fingers is influenced by the material properties and the geometric dimensions of the device structure. All these parameters define the performance, efficiency, and applications of SAW devices in telecommunication, signal processing, and industrial monitoring fields.

The frequency response *(H(f))* of the SAW device is modeled using the impulse response method. The proposed model is a first-order approximation, which neglects second-order effects such as acoustic wave reflections. This approach captures the piezoelectric, electrical, and mechanical characteristics of the SAW device. It is specifically applicable to transducers with unweighted IDTs, assuming a constant finger overlap (aperture) and a metallization ratio of 0.5 μm between the electrodes and the spaces. Using this model, various electrical characteristics such as frequency response, conductance, admittance, impedance, and related performance parameters can be calculated. The impulse response method utilizes the Mason equivalent circuit as its foundational model. In this model, $G_a(f)$ represents for radiation conductance, $B_a(f)$ denotes the acoustic susceptance, and $C_T$ refers to the total capacitance of the system.

The frequency response of the SAW system is modeled using the impulse response method. For a

single IDT, the frequency response is characterized by a *sinc* function and is calculated using the following Eq. (1)[25, 26]:

$$|H(f)| = 2k\sqrt{(Csf_0)N_p}\ \frac{sin(X)}{X}\ e^{\frac{-j2\pi f\ N_p}{2f_0}} \quad \ldots (1)$$

where f represents the frequency, $f_0$ is synchronous or central frequency, *Np* denotes the number of finger pairs, $k$ is the electromechanical coupling coefficient of the piezoelectric material, and $C_s$ corresponds to the capacitance per unit length for a single finger pair. Here, the variable $X$ is introduced for simplifying the equation that is defined as follows:

$$X\ =\ N_P\,\pi\,\frac{(f-f_0)}{f_0} \quad \ldots (2)$$

Admittance (Y): The total admittance is determined by combining total capacitance, acoustic susceptance and radiation conductance. It can be expressed as

$$Y\ =\ G_a + j(2\pi\ fC_T + B_a) \quad \ldots (3)$$

Impedance (Z): The total Impedance as a function of frequency is the reciprocal of the total Admittance (Y). The expression for the total Impedance of a SAW Delay Line is as follows

$$Z(f) = \frac{1}{\left(G_a + j(2\pi f\ C_T + B_a(f))\right)} \quad \ldots (4)$$

Radiation Conductance ($G_a$): The real part of the input admittance is called the radiation conductance. The radiation conductance is also shaped by the sinc function and is found by-

$$G_a(f) = 8k^2C_sW_af_0\,N_p^2\left|\frac{sin(X)}{X}\right|^2 \quad \ldots (5)$$

where $W_a$ represents the overlap height of the fingers or aperture of IDT.

Acoustic Susceptance ($B_a$): The acoustic susceptance represents the imaginary part of the input admittance and models acoustic wave behavior as an electrical performance parameter. It is obtained by applying the Hilbert transform to the radiation conductance and is expressed as:

$$B_a(f) = \frac{G_a(f_0)sin(2X)-2X}{2X^2} \quad \ldots (6)$$

Insertion Loss (*IL*): Calculating insertion loss is crucial for evaluating the performance of electrical systems. In case of SAW devices, the insertion loss varies with frequency and is determined using the susceptance, conductance, and the load resistance $R_g$:

$$IL(f) = -10log\left[\frac{G_a(f)R_g}{\left(1+G_a(f)R_g\right)^2 + \left[R_g\left(2\pi f\ C_T + B_a(f)\right)\right]^2}\right] \quad \ldots (7)$$

The minimum insertion loss occurs for f = $f_0$. Where $f_0$ is the central frequency. Equations (1)-(7) are used for delay line configuration of SAW device with Quartz substrate.

Standard Delay Line configuration geometry: The geometry of the standard delay line configuration is designed in such a way that the height of the substrate is defined to be 3 times the wavelength λ, while the substrate width is determined by the number of IDTs and the width between the IDTs, as shown in Fig. 3.

For Delay Line configuration geometry of IDT plays an important role as shown in Fig. 3, a single IDT structure where the free region has λ /8, while the metalized region has λ /4 geometry size[27]. Since this is a delay line configuration, the distance between two IDTs is also the same as the metallized region. Additionally, h represents the thickness of the IDTs.

A delay line used by SAW sensor in Fig. 4 has the following design specification:

i Synchronous frequency (freq) is 157.9 MHz 158 MHz, and the substrate used is ST-Quartz

iii. The null bandwidth (NBW) is 3.16 MHz, with load and input resistance of 50 Ω.

iii. The capacitance per unit length of the IDT (CS) is 0.503385 pF/cm, and the acoustic velocity (v) is 3158 m/s.

### 3.2 Effect of IDT Electrode Thickness on the Performance Characteristics

The $S_{11}$ characteristic shown in Fig. 5, specifies the effect of variations in the thickness of the interdigital transducer (IDT) from 0.1 to 0.5 µm on the resonant properties of the delay-line surface acoustic wave

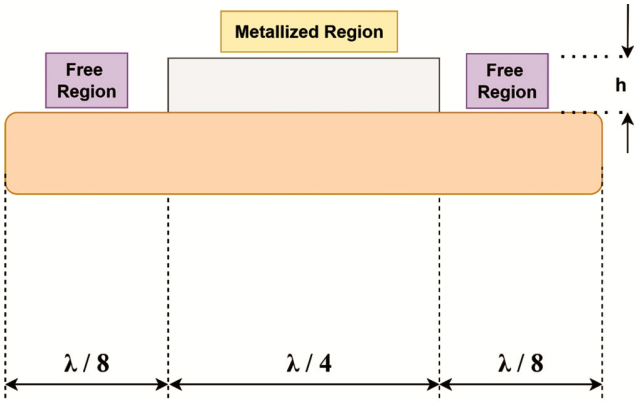


Fig. 3 — IDT's Single Electrode Measurement

(SAW) device designed to operate around 158 MHz. As the electrode thickness increases so does the shift to the left in resonant frequency which at the same time improves return loss. For instance, as the IDT thickness goes from 0.1 μm to 0.5 μm, the resonant frequency goes down from 173 MHz to 151.1 MHz which is a result of increased mass loading and mechanical stiffness of the electrodes which in turn reduces the velocity of the surface acoustic wave which is represented by f=v/λ. Electrode thicknesses in the range of 0.1 to 0.3 μm result in shallow S11 curves with return losses in the range of –1 to –3 dB, thus indicating poor electromechanical coupling and impedance matching. On the other hand, electrodes with thicknesses of 0.4 μm and 0.5 μm result in deep return loss curves with values of about –11 dB, thus indicating increased radiation conductance and acoustic field confinement. A thickness of 0.4 μm results in an optimal response, characterized by a sharp resonance at 158.1 MHz and a return loss of –11.6 dB, thus matching the design frequency of 158 MHz and corresponding to the optimal delay length of 29 μm (1.45λ). This particular value of the delay length reduces electrical feedthrough and spurious reflections, thus improving the efficiency of wave propagation and the quality factor.

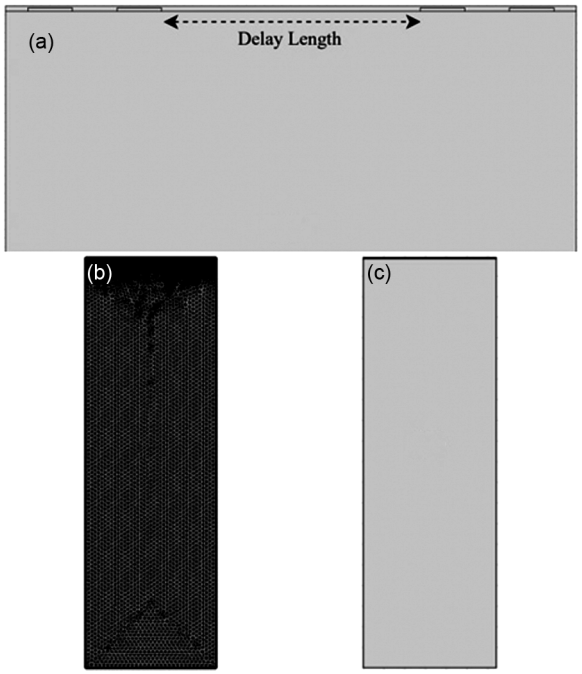


Fig. 4 — Optimized saw sensor geometry with PIB Layer: (a) magnified view of 2D structure, (b) Mesh Geometry, and (c) Complete Geometry

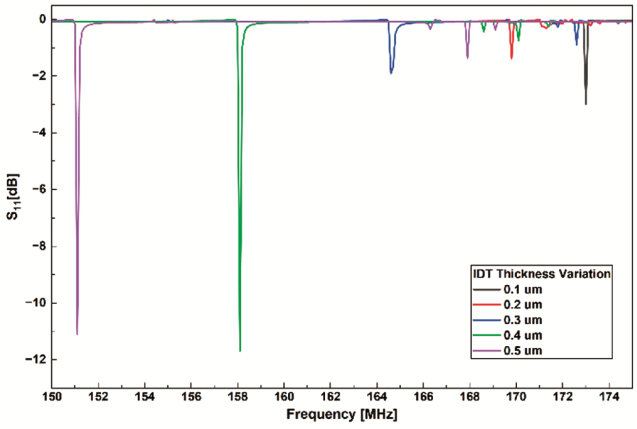


Fig. 5 — Effect of IDT electrode thickness on the frequency response

### 3.3 Effect of IDT Electrode Material on the Performance Characteristics

The effect of electrode material on the performance characteristic is evaluated by changing the IDT material with keeping the 0.4 μm thickness of the IDT electrode. The $S_{11}$ curves shown in Fig. 6, the frequency is shifted due to the varying material properties of the electrodes such as density (ρ), Young's modulus (E), and Poisson's ratio (ν), which affect the mass loading of the electrodes on the piezoelectric substrate. The materials used are Mo (ρ = 10200 kg/m³, E = 312 GPa, ν = 0.31), Au (ρ = 19300 kg/m³, E = 70 GPa, ν = 0.44), Pt (ρ = 21450 kg/m³, E = 168 GPa, ν = 0.38), and Al (ρ = 2700 kg/m³, E = 70 GPa, ν = 0.33). SAW resonates at a frequency given by f = v/λ; the mass loading of the electrodes reduces the acoustic velocity (v) of the SAW on the substrate. Thus, the denser the electrodes, the greater the mass loading effect on the SAW resonator frequency. The highest density of the electrodes is that of platinum at 21450 kg/m³; thus,

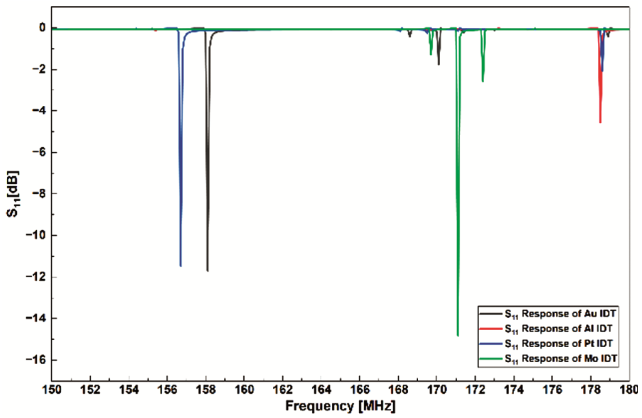


Fig. 6 — Effect of IDT electrode material on the frequency response

platinum exhibits the highest mass loading effect on the SAW resonator frequency, resulting in a resonance at ~157 MHz with a deep $S_{11}$ dip of ~-11 dB. Gold electrodes of slightly lower density at 19300 kg/m³ resonate at a slightly higher frequency of ~158 MHz with a similar return loss depth. Aluminum, with a density as low as 2700 kg/m³, has a minimal mass loading effect, which means that the acoustic velocity remains higher, causing a shift in the resonance frequency to a much higher value, ~178 MHz, with a shallow $S_{11}$ dip of ~–4 dB because of the weaker acoustic confinement. Molybdenum has a unique behavior, with a density lower than that of Au and Pt, at 10200 kg/m³, but with a much higher Young's modulus, 312 GPa, which makes the surface stiffer, thus confining the acoustic wave more efficiently, causing a much deeper $S_{11}$ dip of ~–15 dB at ~171-172 MHz, thus showing a better impedance matching.

This means that while density plays a major role in determining the frequency shift, the Young's modulus also plays a vital role in determining the strength of acoustic wave coupling, with Poisson's ratio also affecting the stress distribution at the interface. The $S_{11}$ curves confirm that both mass loading effects, ρ, and mechanical stiffness, E, play a vital role in determining the resonance frequency, even with constant electrode thickness.

#### 3.4 VOC Sensing Mechanism

Polyisobutylene (PIB) has been chosen as the sensing layer for volatile organic compound (VOC) detection. The physical properties of the gas-sensing layer are summarized in Table 1. As a polymer, PIB is well-suited for VOC sensing due to its high selectivity, permeability, and ability to facilitate rapid adsorption and desorption of analyte vapors. These characteristics contribute to improved reversibility and make PIB an ideal material for gas sensor applications[28]. The main objective of this study is to improve the sensitivity of the SAW sensor for detecting perchloroethylene (PCE) gas.

It is well established that the response of a polymer- coated SAW sensor is directly proportional to the partition coefficient of the analyte in the sensing layer and is given by:

$$\mathrm{k} = \frac{C_s}{C_v} \quad \ldots (8)$$

where $C_s$ is the concentration of the absorbed vapor in the polymer material, and $C_v$ is the total concentration of the vapor in the gas phase.

The absorbed gas reduces the density of the polymer and is given by:

$$\rho_{polymer} + gas = \rho_{polymer} + \Delta\rho \quad \ldots (9)$$

where $\rho_{polymer} + gas$ is the total density of the polymer with absorbed gas, $\rho_{polymer}$ is the density of the polymer, and $\Delta\rho$ is the change in density in the polymer. It is given by:

$$\Delta\rho = kC_vM_{gas} \quad \ldots (10)$$

where $M_{gas}$ is the molecular mass of the gas. $C_v$ is the total volumetric concentration of the gas, expressed as:

$$C_v = N_{ppm}\frac{\delta_{air}}{\mathrm{RT}_{air}} \quad \ldots (11)$$

where $N_{ppm}$ is the gas concentration, R is the gas constant, and $\delta_{air}$ and $\mathrm{RT}_{air}$ are the density and temperature of the air, respectively.

The relationship between the frequency shift ($\Delta f$) and loaded mass ($\Delta m$) in a SAW sensor is expressed as:

$$\Delta f = \frac{2f^2{}_r}{\sqrt{\mu\rho}}\frac{\Delta m}{A} \quad \ldots (12)$$

where μ denotes the elastic constant of the piezoelectric layer, ρ is its density, and A corresponds to the active sensing area of the SAW sensor. The adsorption of the additional mass onto the device surface leads to a shift in the central frequency, with the mass sensitivity defined as

$$S = \frac{\Delta f}{\Delta m} \quad \ldots (13)$$

The VOC gases parameter, VOC gas / PIB partition coefficient and molar mass used for the FEM analysis depicted in Table 2.

Table 1 — The FEM simulation parameters used for PIB Layer

| Parameter | Value for PIB |
|---|---|
| Relative permittivity of PIB | 2.2 |
| Density(kg/m$^3$) | 918 |
| Young modulus (GPa) | 10 |
| Poisson's Ratio of PIB | 0.48 |

Table 2 — The VOC gases parameter used for the FEM analysis

| VOC Gas | VOC gas/PIB Partition Coefficient (k) | Molar Mass of VOC Gas (g/mol) |
|---|---|---|
| PCE | 954.77 | 165.83 |
| TCE | 250.84 | 131.4 |
| $CC_4$ | 160.69 | 153.8 |
| TCM | 84.58 | 119.5 |
| DCM | 30.34 | 85 |

## 4 Results and Discussion

### 4.1 Device Optimization using Finite Element Simulation

This work focuses on choosing the different finger pairs with the different delay lengths to determine the optimal configuration for SAW resonators. Specifically, this finding enables us to identify the saturation point, which represents the maximum number of finger pairs that can be effectively utilized at a particular resonant frequency without generating unwanted harmonic modes.

Substrate plays a very significant role in SAW devices to support the wave propagation and provide mechanical stability and compatibility with microfabrication. Among them, the typical substrates are Quartz, Lithium Tantalate, Lithium Niobate, zinc oxide, langasite, aluminum nitride, and silicon that can support high piezoelectric values to convert electrical signal to acoustic waves.

The choice of substrate has a significant bearing on the major characteristics of the device, including wave propagation, dielectric interaction, and performance in harsh environments or at high-frequency applications[29].

Use of finite element analysis (FEA), Finite Element Analysis is a simulation technique that can be applied for the optimization of the piezoelectric substrate-based Surface Acoustic Wave (SAW) device. The device is then investigated further in detail, including how surface acoustic waves would propagate, interact with elements including transducers and reflectors, and respond to environmental variations. FE analysis is used to perform iteration on designs, optimize waveguide and electrode layouts, and select appropriate configuration. FEA accelerates the design process, guides decision-making, and validates results against experiments, ultimately leading to improved SAW device functionality[30].

The usage of piezoelectric materials is utterly important in the design of a SAW device, so that there are effective wave propagation and performance. The main considerations are material type, crystal orientation, electromechanical coupling factor, thermal expansion, and wave velocity. Piezoelectric materials, in general, exhibit both direct and reverse piezoelectric effects, where mechanical stress is converted into electric charge and vice versa, thus generating SAWs upon the application of alternating voltage. It promotes higher efficiency in coupling, and a low thermal expansion coefficient is desirable except that the sensing elements should have a different thermal expansion coefficient in temperature- sensing devices. A high Q factor is also desirable owing to the presence of low energy dissipation[31].

Devices based on SAW (which includes but is not limited to filters) rely on IDTs in order to generate electromechanical waves on piezoelectric substrates. The design - electrode width, spacing, aperture and count of digits - has to be chosen to maximize the frequency response while minimizing insertion loss. The benefits of delay lines, split electrodes and unidirectional designs are different. Delay lines as shown in Fig. 7 are relatively simple but suffer from wave energy loss; split electrodes reduce reflections and allow higher harmonics.

More complex designs that include DART and floating electrode IDTs continue to improve upon the characteristics by enhancing the frequency response and reducing insertion loss. In the cases of dispersive and tapered IDTs, the electrode dimension is varied for the greater band- width as in focused electrodes, where acoustic energy is focused for specific applications[32]. Generally, IDTs are fabricated from metals such as aluminum, gold, or platinum with their high conductance and mechanical strength; particularly aluminum is used because its adhesion with substrate and preparation is relatively easier than the other materials while also being cheaper.

By this experimentation, a proper balance was found which gives efficient wave transmission while

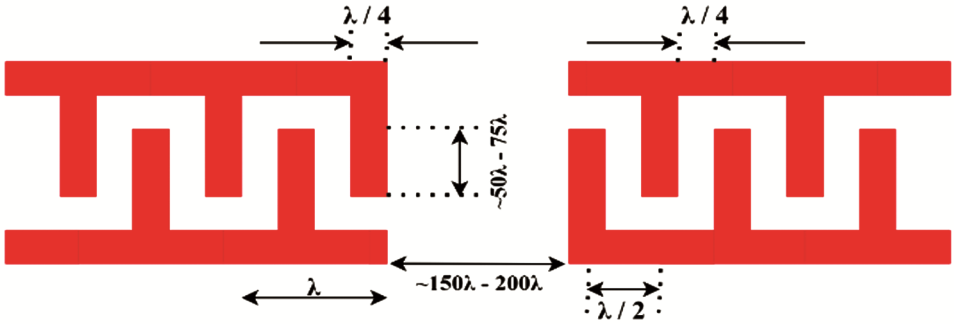


Fig. 7 — Delay Length Configuration of the IDT

minimizing energy loss. The addition of more electrodes has allowed finer control over acoustic waves, which has dramatically improved signal processing capabilities in the case of the SAW filter. This FEA simulation provided insight into how to balance the delay line configuration that may further optimize the overall performance and efficiency of the device. The delay length was approximately set to about 29 µm for 1.45λ.

The geometry of a SAW device is setup via the model builder sidebar in the design workbench by setting its height and width to predefined values. Here, the thickness of IDTs is fixed at 5 µm while the total width of the substrate is 40 µm with a 5 µm gap between IDTs. The substrate for this design was assigned to quartz, while the IDTs were made of gold. After determining the geometry, terminal, ground, and floating potential conditions are applied to obtain mesh analysis. Finally, frequency domain analysis is performed to see how the device behaves.

For a mode to be electrically detectable by interdigitated transducers (IDTs), it must possess a non-zero net electrical potential or charge distribution that interacts with the IDT electrodes, allowing for efficient electromechanical coupling. FEM-based COMSOL simulations inherently capture this electromechanical coupling. The modes presented are those that exhibit significant displacement profiles under the IDTs, indicative of strong coupling and thus electrical detectability.

The simulation setup, including the defined boundary conditions, is designed to accurately model the electromechanical behavior of the piezoelectric material and the IDTs, ensuring that the identified modes are indeed those that would be excited and detected by the electrical ports. It has been verified that the modes corresponding to the $S_{11}$ dips exhibit the necessary displacement and charge patterns consistent with electrical excitation.

Thus, the optimized SAW device as shown in Fig. 4 is achieved with optimized delay length of 1.45 λ or 29 µm, highly increasing wave propagation efficiency and reducing insertion loss significantly. Overall, this increases performance over compared earlier designs, giving better acoustic signal integrity and overall functionality to the device. This optimized SAW device has been utilized for the gas sensing application. For sensor application, avoid the utilization SAW device with larger number of pair. Due to the increase of higher harmonic mode and spurious mode for the larger number of electrode pair. Comparing the performance metrics, an updated SAW device with a delay length of 1.45 λ (29 µm) has better performance metrics. From the displacement plot in Fig. 8, it was seen that for this SAW device better energy transfer with very minimal wave interference, and hence acoustic integrity in a signal will be improved.

The displacement plot in Fig. 8 shows a sharp peak at about 158 MHz, which implies that it is the resonant frequency of the SAW device where maximum displacement occurs. This peak, therefore, means efficient energy transfer and optimal wave propagation at that frequency as the SAW device experiences its maximum displacement amplitude. Beyond this frequency, displacement values are lost rapidly, hence illustrating that the device is narrowband. This sharp resonance behavior indicates good tuning of the SAW device so that it will work at the desired frequency with minimum energy loss.

The admittance plot from Fig. 9 provides the $Y_{11}$ parameter in dB, meaning how efficiently the SAW device conducts energy at the different frequencies. The peak around the resonant frequency suggests the maximum admittance-that is, a minimum impedance and optimal energy transfer. This behavior is in conformity with the optimal delay length designed to optimize wave propagation. As the frequency moves away from the resonant point, admittance decreases, thus increasing the impedance and the efficiency of the device. Such a plot would help confirm at what frequency the SAW device is the most efficient and would also highlight design optimizations on the device performance.

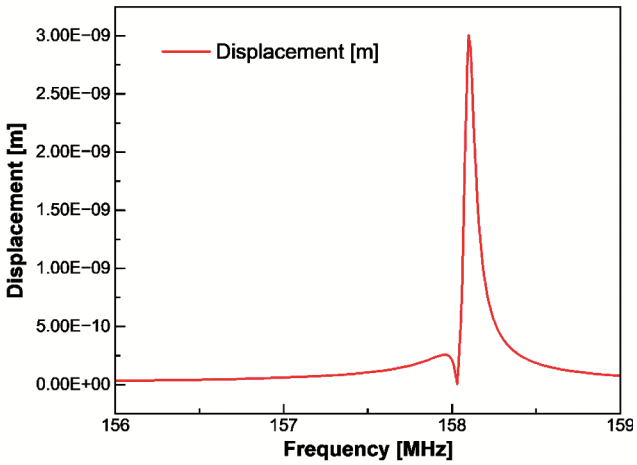


Fig. 8 — Displacement Plot for the Optimized SAW Device

The $S_{11}$ plot shown in Fig. 10 shows a significantly reduced signal reflection and therefore lower insertion loss. The frequency response of the proposed device, thereby is highly improved with optimized reflection characteristics and enhanced operation efficiency. The extracted performance parameters of the optimized SAW resonator had acoustic wave velocity of 3158 m/s, center frequency of 158.39 MHz, and quality factor of 2635.

For SAW resonator, the quality factor (Q) is expressed as follows:

$$Q = \frac{f_0}{\Delta f_{3dB}} \quad \ldots (14)$$

where $f_0$ is the central frequency of the resonator and $\Delta f_{3dB}$ is the 3dB bandwidth of the resonator. For a free, damped harmonic oscillator, Q is defined as the ratio of the energy stored in the oscillation to the energy dissipated per cycle due to damping, i.e.,

$$Q = 2\pi \left( \frac{Energy\ Stored}{Energy\ Dissipated\ per\ Cycle} \right) \quad \ldots (15)$$

The energy in such a system decay exponentially over time as $E(t) = E_0 e^{-\alpha t}$. Here, $E_0$ is the initial energy and $\alpha$ is the damping coefficient (or decay rate), which is related to the energy dissipated per cycle. The bandwidth $\Delta f_{3dB}$ is also related to this damping factor. A simple mathematics leads to $Q \approx \frac{\omega_0}{2\alpha}$, (where $\omega_0 = 2\pi f_0$), which can then be shown to be equivalent to $f_0/\Delta f_{3dB}$ for a high-Q system, which is a widely accepted and practical approximation.

The reported Q value of 2635 was obtained under idealized conditions with no loss mechanisms modelled. Q is defined as a ratio; in practice the inclusion of loss mechanisms does matter. Loss mechanisms, such as material damping, electrode resistance, or other parasitic effects, tend to increase the 3 dB bandwidth, $\Delta f_{3dB}$, because they introduce additional damping. Even though the central frequency $f_0$ might remain largely unchanged, a broader bandwidth in the presence of losses results in a lower Q value.

Therefore, while the form of the ratio does not change, the numerical result is significantly affected by whether or not loss mechanisms are incorporated. Considering the ideal scenario, the estimate of the intrinsic performance of the SAW resonator is provided. It is worth noting that in a practical device where these losses cannot be neglected, the quality factor would indeed be lower. Hence, this comparatively higher Q = 2635 could be ascribed as an upper-bound performance estimate.

The delay length is adjusted to optimize the SAW device to increase wave propagation along with reduced signal reflection. A quartz substrate with gold electrodes was used along with various analysis, which include displacement, stress distribution analysis, and analysis on $S_{11}$. Further, the analysis on $S_{11}$ also showed lower reflection with more acute response. An optimized design had a delay length of 1.45 λ and was peaking at a resonant frequency of 158.12 MHz before introducing PIB layer.

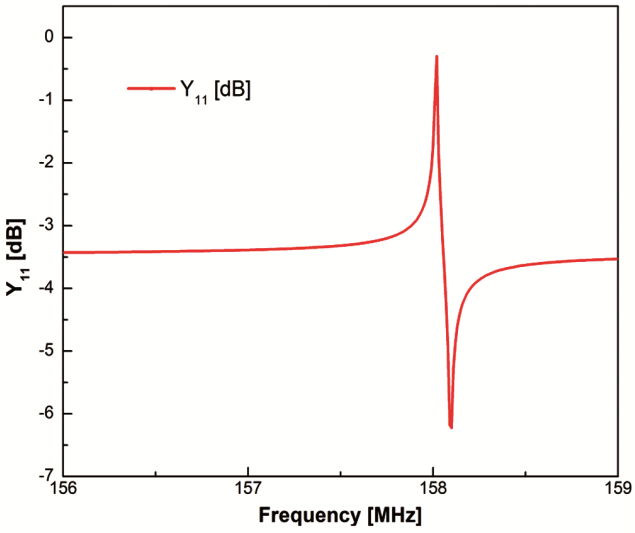


Fig. 9 — Admittance Plot for the Optimized SAW Device

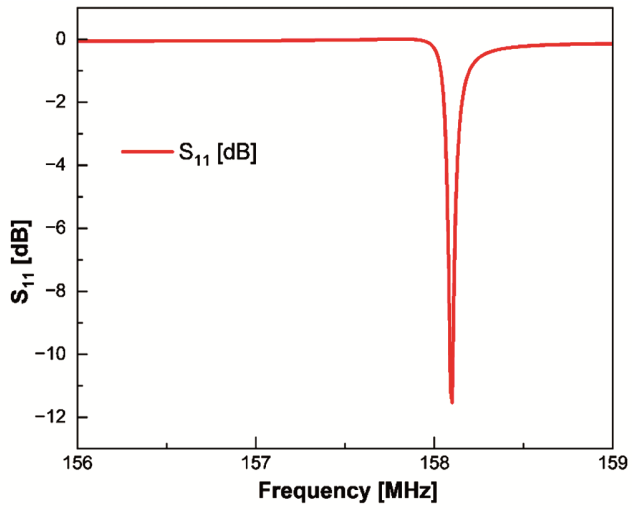


Fig. 10 — $S_{11}$ Plot for the Optimized SAW device

#### 4.2 Effect of PIB Sensing Layer Thickness

To evaluate the impact of PIB layer thickness on device sensitivity, the SAW sensor was designed with varying PIB thicknesses. As shown in Figs. 11 (a-c),

thicknesses of 0.45 µm, 0.5 µm and 0.6 µm were tested. The results indicate that the frequency shift increases with thicker PIB layers, leading to enhanced sensitivity of the PCE gas sensor as the PIB layer thickness grows.

Sensitivity of the Optimized SAW Sensor is defined by using results obtained from Fig. 11. The optimized SAW sensor has further been researched based on results received that after deployment of PIB layer 0.6 µm the sensor resonates at 158.39 MHz. It displays the dynamic sensing of optimized SAW when exposed to variable concentrations of the PCE gas. The sensitivity for 0.45 µm, 0.5 µm and 0.6 µm is observed to be 0.38 kHz/ppm, 0.48 kHz/ppm and 0.67 kHz/ppm, respectively.

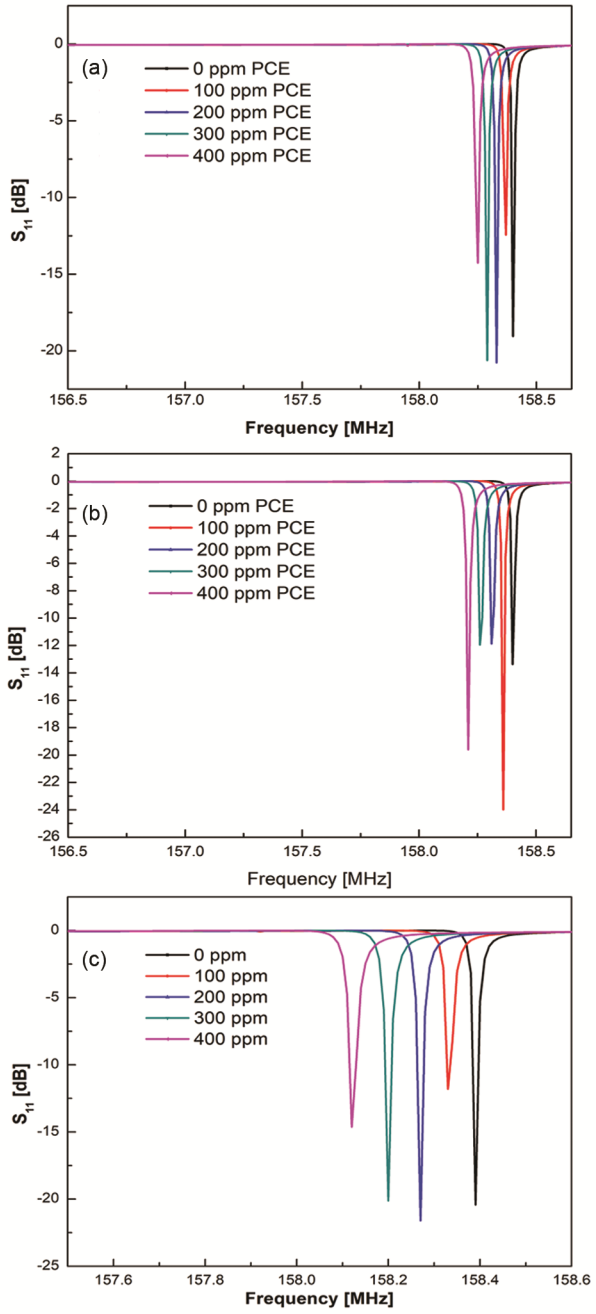


Fig. 11 — (A) PCE gas sensor response for 450 nm thick PIB layer. (B) PCE gas sensor response for 500 nm thick PIB layer. (C) PCE gas sensor response for 600 nm thick PIB layer

Figure 12 illustrates the variation in resonant frequency as a function of PCE gas concentration for different PIB layer thicknesses. These trends are consistent with the simulation results presented in Fig. 11. The PCE sensor with a 0.6 µm PIB coating exhibited the highest sensitivity of 0.67 kHz/ppm. The possible detection limit (LOD) of the proposed SAW sensor is given[33].

$$LOD = \frac{3\sigma}{Sensitivity} \quad \ldots (16)$$

where σ is the average noise of the central frequency of the SAW sensor without adsorption of the gas. The calculated LOD of the PCE gas sensor was about 2.42 ppm for the average noise of 0.54 kHz. When the SAW sensor is exposed to PCE gas, the PIB film selectively adsorbs the gas from the surrounding atmosphere, resulting in the increased mass loading. The Finite Element Method (FEM) simulations were performed for different PCE gas. concentrations, which alter the density of the PIB thin film (Δρ) due to gas adsorption.

#### 4.3 Sensitivity and Selectivity Analysis for VOC Detection

Selectivity study of the SAW sensor towards PCE gas was performed by simulating the sensing response in the presence of interfering gases with high concentration 400 ppm as shown in Fig. 13. It is clearly seen from

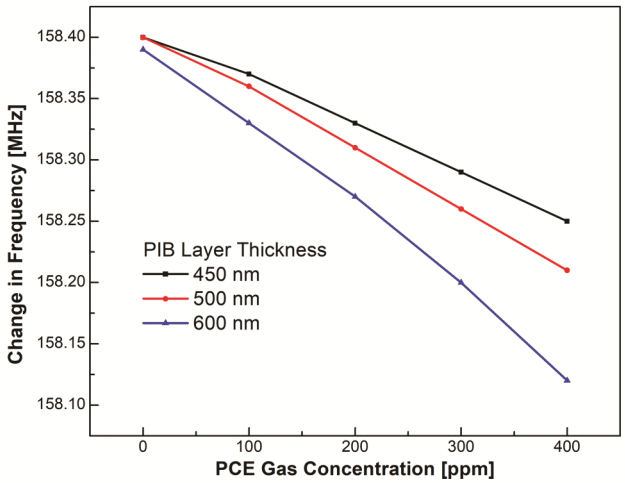


Fig. 12 — Change in resonant frequency with a change in concentration of PCE gas for different thicknesses of the PIB layer

Fig. 13 that, shift in resonant frequency of SAW sensor is higher for PCE gas while other interfering gases show minor shift.

The simulated results clearly show that the delay Line based SAW sensor is highly sensitive and selective towards PCE gas at room temperature. For saturating value was seen with high concentration level being more than 400 ppm since the number of adsorbing sites by a PIB layer is relatively finite. As illustrated in Fig. 13, the frequency downshift of the SAW sensor was linear with the concentration of PCE gas before it reached saturation, with a regression coefficient ($R^2$) of 0.9861. The gas sensitivity, as defined as the slope of the calibration curve, was calculated to be 0.67 kHz/ppm within the linear response range for 0.6 µm PIB layer.

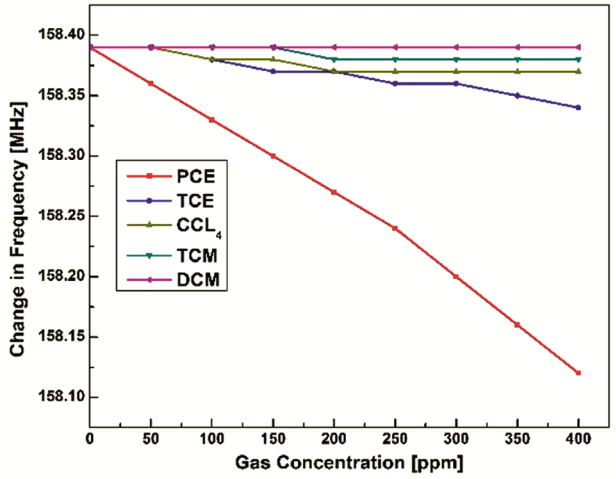


Fig. 13 — Frequency shift of the SAW sensor as a function of gas concentration for various analytes (PCE, TCE, $CCl_4$, TCM, and DCM)

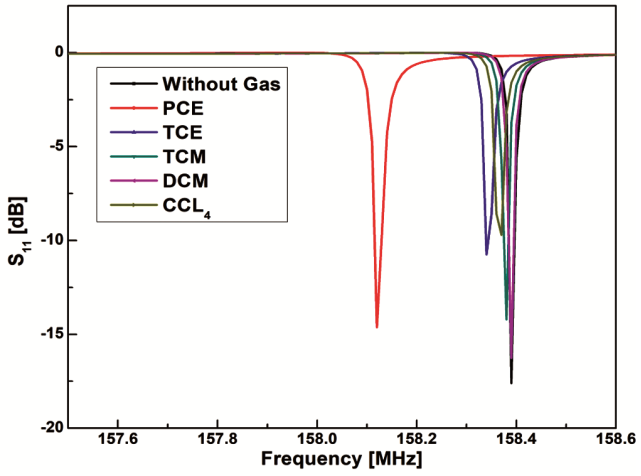


Fig. 14 — Sensing response in the appearance of interfering gases with high concentration 400 ppm

For mass-loading sensors, working at higher frequency enhances the frequency shift per unit mass change. This implies that the SAW sensor exhibits a gas sensitivity about an order of magnitude greater than that reported for conventional QCM-based sensors. Interestingly, the SAW sensor functions effectively at room temperature, and it is therefore very suitable for practical applications. It is observed from Table 3 that the sensitivity of PCE gas is more because of its high density and more molar mass as compared to other VOC gases.

Unlike the MOS and CNT sensors[34] that depend on the analog resistance or current signals, the SAW sensor relies on a digitized frequency response that is more robust and does not require analog-to-digital conversion. The fabrication at the micrometer scale, and compatibility with MEMS technology, allows an electronic nose to be developed through the integration of multiple SAW sensors with various polymer coatings. Every sensor responds uniquely to the different analytes and is then possible to generate a pattern of a fingerprint for gaseous accurate identification in complex environments. As an illustration, in Fig. 13, the SAW sensor gave differential responses for PCE, TCE, $CCl_4$, TCM, and DCM gases, as it would be indicative for specific kinds of detection of volatile organic compounds. In addition, the dynamic response of the optimized SAW sensor to various gas analytes is shown in Fig. 14.

The $S_{11}$ parameter shows different frequency shifts when exposed to different gases, such as PCE, TCE, TCM, DCM, and $CCl_4$, compared to the baseline (without gas) at 400 ppm concentration. Among them, PCE shows the highest frequency shift, which indicates a higher simulated adsorption affinity with the sensing layer.

The different gases had varying resonance frequency, thus implying the selectivity of the SAW sensor that would be used in differentiating several volatile organic compounds. The observed shifts confirmed the capability of the sensor in detecting and

Table 3 — The frequency shifts and sensitivity in exposure to VOC Gases at 400 ppm concentration

| Gas Exposure | Frequency Shift (kHz) | Sensitivity (S) (kHz/ppm) |
|---|---|---|
| PCE | 270 | 0.67 |
| TCE | 50 | 0.123 |
| $CCl_4$ | 20 | 0.057 |
| TCM | 10 | 0.033 |
| DCM | 0 | 0 |

Table 4 —The comparison of VOC gas sensor reported in the literature

| Reference | VOC Gas | Type of Device | Resonance Frequency ($f_r$) MHz | Sensitivity (S) (kHz/ppm) |
|---|---|---|---|---|
| This work | PCE | SAW | 158.39 | 0.67 |
| [35] | PCE | SAW | 1167 | 0.012 |
| [35] | PCE | SAW | 1200 | 0.025 |
| [36] | DCM | SAW | 842.9 | 0.002 |
| [37] | DCM | SAW | 104 | 0.038 |
| [37] | DCM | SAW | 208 | 0.152 |
| [38] | DCM | SAW | 855.47 | 0.0028 |

quantifying the concentrations of the gas in the air effectively and suitable for environmental and industrial monitoring applications.

The Table 4 indicates the comparison of the sensitivity of different SAW devices for VOC gas sensing, i.e., PCE and DCM, at different frequencies. The SAW device at a frequency of 158.39 MHz has the greatest sensitivity of 0.67 kHz/ppm, with large frequency shift per ppm of PCE gas. The comparison clearly indicates that the delay line plays a significant role in improving the sensitivity of the SAW sensor.

## 5 Conclusion

In conclusion, a finite element analysis-based optimization of SAW resonator structures by varying delay lengths is presented. The quality factor (Q) was calculated using the 3 dB bandwidth method under idealized, lossless conditions. While this results in a comparatively high Q value of 2635, it serves as an upper- limit estimate of intrinsic device performance. Practical devices would inevitably experience reduced Q due to material damping and other parasitic effects. The optimized SAW resonator, operating near 158.39 MHz, was used for VOC gas sensing. Frequency-domain simulations show a linear frequency downshift with increasing concentrations of PCE gas, achieving a sensitivity of 0.67 kHz/ppm for a 600 nm PIB sensing layer. This response surpasses many previously reported SAW sensors. Additionally, the variation in $S_{11}$ responses across multiple analytes demonstrates the sensor's selectivity, an essential property for practical multi-gas detection platforms. While this work is simulation-driven, the findings provide a strong foundation for experimental validation and pave the way for developing compact, selective, and high-performance SAW-based VOC sensors for industrial and environmental monitoring.

## References


1 Turuk B K & Behera B, *Eng Res Express*, 6 (2024) 022302.

2 Feng Y, Li J, Bai R & Qian Z, *IET Circuits, Devices Syst*, 16 (2022) 483.

3 Wang, Tianran, Yuanxun Xia & Yifan Li, *Micromachines*, 14 (1) (2023) 106.

4 Shevchenko S Y & Mikhailenko D A, *Sensors*, 22 (3) (2022) 1142.

5 Kumar R & Mandal N, *IEEE Sensors J*, 24 (2024) 5713.

6 Fernández-García A, Solís-Tinoco V I, Arce M a A, Villa-Vargas L A, Salinas M A R & García J C S, *Int J Numerical Model: Electron Network, Devices Fields*, 37 (2024) e3306.

7 Vinita, Pareek D, Kumar Gupta S & Singh J, *IEEE Sensors J*, 24 (2024) 31932.

8 Singh J, Gupta S K & Vinita, *Sensors Actuators A: Phys*, 365 (2024) 114818.

9 Kumar P, Singh J & Kaur D, *IEEE Sensors J*, 24 (2024) 2664.

10 Abraham N, Reshma Krishnakumar R, Unni C & Philip D, *J Sci: Adv Mater Devices*, 4 (2019) 125.

11 Pasupuleti K S, Chougule S S, Vidyasagar D, Bak N h, Jung N, Kim Y H, Lee J H, Kim S G & Kim M D, *Nano Research*, 16 (5) (2023) 7682.

12 Pasupuleti K S, Pham T M T, Abraham B M, Thomas A M, Vidyasagar D, Bak N H, Kampara R K, Yoon S G, Kim Y H & Kim M D, *Adv Composite Hybrid Mater*, 8 (1) (2025) 132.

13 Anbalagan S, Lakshminarayanan S & Girija K G, *Physica Scripta*, 99 (2024) 075970.

14 Qureshi S, Hanif M, Jeoti V, Stojanovic´ G M & Khan M T, *Results Eng*, 22 (2024) 102323.

15 Hossain N, Mahmud M Z A, Hossain A, Rahman M K, Islam M S, Tasnim R & Mobarak M H, *Result Eng*, 22 (2024) 102115.

16 Samanta A & Roy S, *Phys Rev Appl*, 22 (5) (2024) 054076.

17 Samanta A & Roy S, *IEEE Trans Electron Devices*, 70 (2023) 335.

18 Morankar A & Patrikar R, *IET Circuits, Devices & Syst*, 12 (2018) 88.

19 Kumar P, Vinita, Pawar S, Singh J & Kaur D, *IEEE Electron Device Lett*, 43 (2022) 446.

20 Bharati M, Rana L, Gupta R, Sharma A, Jha P K & Tomar M, *Optic Mater*, 142 (2023) 114088.

21 Rana L, Gupta R, Sharma A, Tomar M & Gupta V, *IEEE Trans Electron Devices*, 65 (2018) 1523.

22 Patel R, Patel M, Boolchandani D & Rangra K, J Micro/Nanolithograp, MEMS, and MOEMS, 16 (2017) 025002.

23 Bharati M, Rana L, Gupta R, Sharma A, Jha P K & Tomar M, *physica status solidi (a)*, 220 (2023) 2200760.

24 Wang T, Green R, Guldiken R, Wang J, Mohapatra S & Mohapatra S S, *Sensors*, 19 (2019) 1749.

25 Wilson W C & Atkinson G M, 1st Order Modeling of a SAW Delay Line using MathCAD, ® *IEEE SoutheastCon*, 2007 pp. 1–6.

26 Wilson W C & Atkinson G M, *IEEE Int Behav Model Simulation Workshop*, (2006) pp. 34–39.

27 Yang S, Ai Y, Zhang Y, Cheng Z, Zhang L, Jia L, Dong B, Zhang B & Wang J, *J Micromechanic Microeng*, 28 (2018) 085005.
28 Panchal B, Bhadauria A & Varghese S, *Fractal Fractional*, 6 (2022) 491.
29 Slobodnik A, *Proceed IEEE* 64 (1976) 581.
30 Mandal D & Banerjee S, *Sensors*, 22 (2022) 820.
31 Chen P, Li G & Zhu Z, *Micromachines*, 13 (2022) 656.
32 Campbell C & Burgess J C, *J Acoustical Soc America*, 89 (1991) 1479.
33 Chen D, Yang L, Yu W, Wu M, Wang W & Wang H, *Micromachines* 9 (2018) 62.
34 Guz, Łukasz, *MATEC Web Conf,* 252 (2019) 06007.
35 Aslam M Z, Jeoti V, Karuppanan S, Malik A F & Iqbal A, *Sensors*, 18 (2018) 1687.
36 Ionescu V, *Romanian J Phys*, 60 (3) (2015) 502.
37 Achour B, Attia G, Zerrouki C, Fourati N, Raoof K & Yaakoubi N, *Sensors*, 20 (2020) 4994.
38 Moustafa M, Laouini G, ElNaggar M & AlZoubi T, *Ferroelectrics*, 572 (2021) 94.